ORIGINAL PAPER

CrossMark

The Mild-Severe Wear Transition in Erosion Wear

O. A. Zambrano[1] · D. S. García[1] · S. A. Rodríguez[1] · J. J. Coronado[1]

Abstract

In this study, three types of abrasives and several types of heat treatments and materials were used to obtain 11 different abrasive/material hardness (H_a/H_m) ratios with the aim of elucidating the effect of the H_a/H_m ratio on the mild-severe wear transition in erosion wear. This effect has seldom been addressed in the erosion wear literature focused on metallic materials. Solid particle erosion wear tests were performed. The experimental results showed different wear regimes when the H_a/H_m ratio was modified based on the fracture toughness of the erodent material (K_{Ic}); a moderate wear regime was observed for modified $H_a K_{Ic\_abrasive}/H_m$ ratios less than 2, while a severe-moderate transition was observed for values between 2 and 4. The wear surface observations revealed a relationship between the wear erosion regimes and the wear micromechanisms. For the moderate wear regime, only superficial grooves and a slight plastic deformation were observed; for the transition wear regime, deeper grooves and craters were observed. Finally, in the severe wear regime, the deepest grooves and craters were observed, as were plastic deformation and cutting.

Keywords Erosion wear · Mild-severe wear transition · Hardness ratio · Steel · Wear micromechanisms

1 Introduction

In the erosion wear literature, the effects of factors such as impact velocity [1], impact angle [2–4], particle concentration [5, 6], strain hardening of the material surface [4], particle size [7, 8], impact-induced phase transformation [9], and particle morphology [10] have been systematically studied with the aim of obtaining a broad understanding of this phenomenon. Evidently, the properties of a material are also involved in the wear response; for instance, erosive wear differs considerably between materials with predominantly brittle and ductile behaviors. Brittle materials tend to lose more mass when subjected to impact at high angles, and ductile materials tend to lose more mass when subjected to impact at low angles [11]. This phenomenon is controlled by fracture toughness, which is intimately related to material hardness. For instance, Evans et al. [12] examined the influence of fracture toughness and hardness on brittle materials and revealed that material removal is inversely proportional to both the fracture toughness and hardness raised to an odd

exponent. However, in an tribosystem with erosion, not only the aforementioned variables but also other factors, such as the ratio of the abrasive hardness (H_a) to the material hardness (H_m), are important. The H_a/H_m ratio drastically influences the erosion wear response, mainly because this relationship implicitly involves several of the aforementioned properties. To a certain degree, the H_a/H_m parameter may be considered a first approach and a basic tool in reproducing an industrial or practical situation at the laboratory scale. This parameter facilitates the replication of a similar wear regime when other parameters are difficult to scale.

The H_a/H_m parameter has been used to study the wear behavior of different alloys under abrasive conditions, leading to the identification of wear transition regimes [13, 14]. However, studies of erosion wear are scarce. Some important contributions were made by Wada et al. [15] and Feng et al. [16], who showed that a proportional relationship between the erosion rate and the H_a/H_m ratio exists for ceramics; these authors observed, in general, that an increase in the H_a/H_m ratio produces a drastic increase in the wear rate. In ductile materials, the effect of the H_a/H_m ratio on erosion wear has been rarely studied. One of the few such analyses was performed by Desale et al. [17], who mixed solid particles and water at a velocity of 3 m/s and identified three main regimes in which the erosion wear rate was a function

✉ J. J. Coronado
john.coronado@correounivalle.edu.co

[1] Research Group of Fatigue and Surfaces (GIFS), Mechanical Engineering School, Universidad del Valle, Cali, Colombia

of the H_a/H_m ratio: in the region of moderate wear, H_a/H_m was between 4.2 and 5.2; in the region of intermediate wear, H_a/H_m varied from 6.9 to 12.1; and in the severe wear region, H_a/H_m varied from 12.5 to 27.5. However, a systematic study of H_a/H_m ratios from 1 to 5, which are typically observed under industrial conditions with low erodent particle sizes and high velocities, such as in hydraulic turbines, has not yet been performed; this type of systematic study is one of the main contributions of the present work.

The main goals of this work were to study the erosion wear phenomenon for materials as a function of the H_a/H_m ratio and to determine whether a mild-severe wear transition exists under the erosion test conditions. Three different abrasives were used: silica sand, aluminum oxide (Al_2O_3), and garnet. The erosion wear tests were performed on the following six materials with different hardnesses: cemented carbide, AISI DF2, AISI D2, AISI D3, and AISI M2 tool steels, and AISI 420 stainless steel. Most of these materials were subjected to different heat treatments to achieve the required hardness, with the exception of the cemented carbide and AISI D2. These conditions allowed us to evaluate 11 different H_a/H_m ratios and their effects on erosion wear.

2 Experimental Procedures

2.1 Abrasives

Special care was taken to avoid the influence of the abrasive particle size and particle morphology on the results of the erosive wear tests. To accomplish this, three abrasives were used: Al_2O_3, garnet, and river sand. Abrasives with the most similar particle size and morphology were acquired; in the case of the river sand, several cycles of sieving were necessary to obtain the adequate particle size in the amount required to perform the tests. The silica sand was extracted directly from the Amaime River (Palmira, Colombia). The density of the erodent might also be an important feature in erosion wear since the hardness of similar particles (same size and morphology) could induce different wear behaviors due to the various resultant momentum transfers to the material surface. For the aforementioned reasons, the morphology, size, and density of the particles were measured.

Notably, the morphology of the particles can be characterized through the shape factor, which allows a dimensionless value of roundness to be obtained using particle characteristics, such as projected area and perimeter, from many particles. Therefore, the following procedure was used for particle morphology characterization. Approximately 1 g of each sample was extracted; the samples were dispersed over a glass surface to separate the particles, and a Nikon SMZ1000 micro-stereoscope was used to take several photographs at $120\times$ magnification. On average, 6 photographs

were taken per sample, and each photograph captured between 15 and 25 particles. Afterward, the images were processed using the free, open-source ImageJ software, as shown in Fig. 1.

The area (pixels^2) and perimeter (pixels) of the particles were determined and subsequently used to calculate the shape factor SF using Eq. (1), as originally proposed by Cox [18]. However, the standard deviation of the shape factor for the abrasives used in this study might be large; therefore, the modified shape factor [2] was used, as shown in Eq. (2), with the aim of improving the statistical significance of the results.

$$SF = \frac{4\pi A}{P^2} \tag{1}$$

$$SF_{Mod} = \left(SF_{mean}\ SF_{min}\ SF_{max}\right)^{1/3} \tag{2}$$

where A is the area of a single particle (projected area in pixels^2); P is the total perimeter (in pixels) of the projected abrasive particles; SF_{mean} is the mean shape factor; SF_{min} is the minimum shape factor, and SF_{max} is the maximum shape factor. The shape factor in this case is related to the "roundness concept," that is, the shape factor represents the percentage ratio of the area of the particle to the area of a circle with the same perimeter, as proposed by Cox.

The commercial availability of certain particle sizes and the range of particle sizes that are applicable to the practical erosion wear of industrial turbomachinery led us to conclude that the abrasive particle sizes should be between 212 and 300 µm. The upper limit of the particle size was chosen based on the desander or sand removal equipment that is usually used in energy plants and that controls the maximum particle size entering the runner [19]. To characterize the size of the abrasives, 300 g of each abrasive was passed
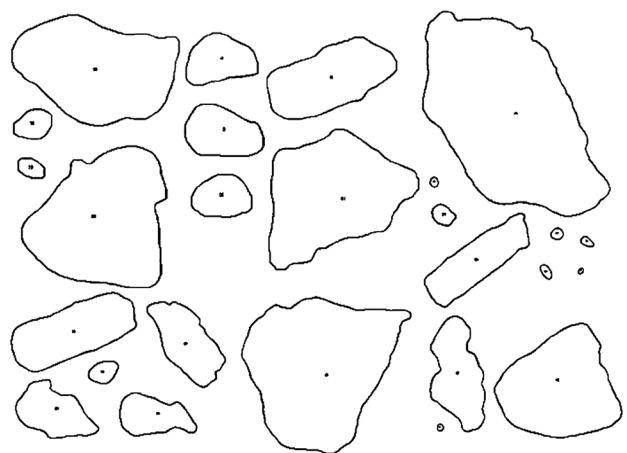

Fig. 1 Examples of the contours of some abrasive particles, obtained using the ImageJ software

through various sieves ranging from 10 to 300 μm. Subsequently, the amount of abrasive that was retained in each sieve was weighed. For the tests, only particles retained in the 212 μm sieve were used. To evaluate the change in particle size before and after the wear test, 100 g of each abrasive was dried in a furnace at 100 °C for 2 h and then sieved through finer meshes and weighed. This process allowed the construction of granulometry curves after the erosion test and evaluation of the fragmentation of the abrasives.

Graduated cylinders and water were used to determine the density of the abrasives. First, 50 ml of each abrasive (apparent volume) was added to a test cylinder. Then, the weight of this abrasive volume was measured. Afterward, 50 ml of water was added to the test beaker to replace the air and fill the voids. This allowed the true volume of the abrasives that were inside the graduated cylinder, i.e., the volume without any void spaces between the particles, to be calculated using Eq. (3).

$$V_t = V_w + V_a \tag{3}$$

where V_t is the total volume (cm^3); V_w is the volume of water, and V_a is the volume of the abrasive. Then, the density (g/cm^3) was calculated using Eq. (4).

$$\text{Density} = \frac{M_a}{V_a} \tag{4}$$

where M_a is the mass (g) of the abrasive.

The particles were cold-mounted in resin, then ground with 1500-grit sandpaper and mechanically polished using 1, 0.3, and 0.05 μm alumina. The particle hardness was determined using a micro-Vickers indenter at 200 gf for 15 s for the Al$_2$O$_3$ and garnet and at 10 gf for 15 s for the silica sand. The test errors were determined based on 10 indentations with 95% confidence.

2.2 Materials

The erosion wear tests were performed on commercial stainless steel AISI 420, four high-speed steels, namely, AISI M2, AISI D2, AISI D3, and AISI DF2, and a cemented carbide.

A Rockwell hardness tester (brand TIME) was used to measure the samples after they were cold-mounted in resin and then ground with 400 grit sandpaper. A diamond conical indenter with a load of 150 kgf was used to test the hardness. The Rockwell C hardness (HRC) values were converted to the Vickers scale using the ASTM E140-12b^{ε1} standard. The test errors were determined based on five indentations with 95% confidence.

The heat treatments were carefully designed to obtain a very specific hardness that allowed us to obtain the required H_a/H_m ratio. The heat treatments used to obtain these specific hardness values are discussed below.

Time-temperature-transformation (TTT) diagrams of each steel were employed following the procedures described in [20]. In summary, the AISI 420 steel was heated at a rate of 197 °C/h to a temperature of 1025 °C with 4 h of holding time and then quench-cooled in oil. Then, the material was tempered at a rate equal to the previous heating rate until the steel reached a temperature of 557 °C; the material underwent a final cooling inside the furnace. For the AISI D3 steel, a simple quenching was required. The AISI D3 specimens were first cut to the required size and then placed into an oven and heated at a rate of 197 °C/h until a temperature of 1010 °C was reached; this temperature was held for 3 h. Finally, the samples were quenched in oil. For the AISI DF2 steel, cut samples were heated at a rate of 180 °C/h until a temperature of 820 °C was reached; this temperature was held for 2 h, and then the samples were quenched in oil. Afterward, two tempering treatments were performed with the same heating rate of 197 °C/h until a temperature of 550 °C was reached; the final cooling took place inside the furnace. The AISI D2 and AISI M2 steels and the cemented carbide did not require any heat treatment because the initial hardness values of these materials were within the desired hardness range.

2.3 Wear Tests

An erosive tribometer was used to perform the solid particle erosion wear tests. A schematic representation of the equipment is shown in Fig. 2. The slurry is fed into an air stream.

The equipment was designed to feed abrasive particles into a high-velocity fluid stream, i.e., air enters the tank to generate the agitation necessary for the slurry mixture (to avoid the settling of particles onto the bottom of the tank). Then, the slurry is pushed upward in the apparatus; the slurry mixes with the air stream (~ 90%), which propels the slurry against a specimen surface oriented at 90° to the 5-mm-diameter ceramic nozzles. This configuration was used to achieve a velocity field similar to that occurring in hydraulic turbines. The fluid mixture contained abrasive in water at a concentration of 1.25 mass%. To achieve the appropriate concentration in the fluid mixture, 8 l of water with 100 g of abrasive was used. Each specimen had a diameter of 16 mm and thickness of 10 mm. The equipment included a loading tank, hose connectors, a Venturi nozzle holder, a pressure reducer, and a pressure gauge. Compressed air was used to agitate the water and abrasive mixture during the test to prevent particles from settling in the tank and to maintain the pressure necessary for the jet. For all the tests, the erodent was not recycled; that is, new abrasives were always used for each test and repetition. The mean jet velocity was estimated to be 100 m/s using computer fluid dynamics (CFD) and biphasic simulations performed in the commercial

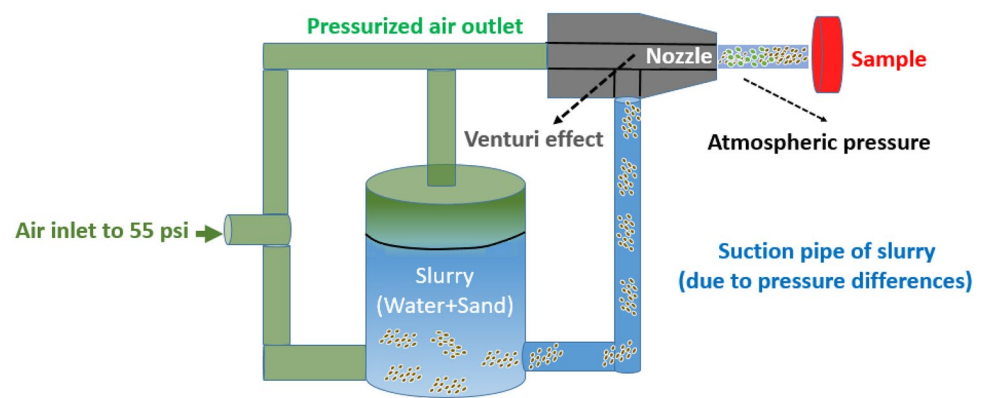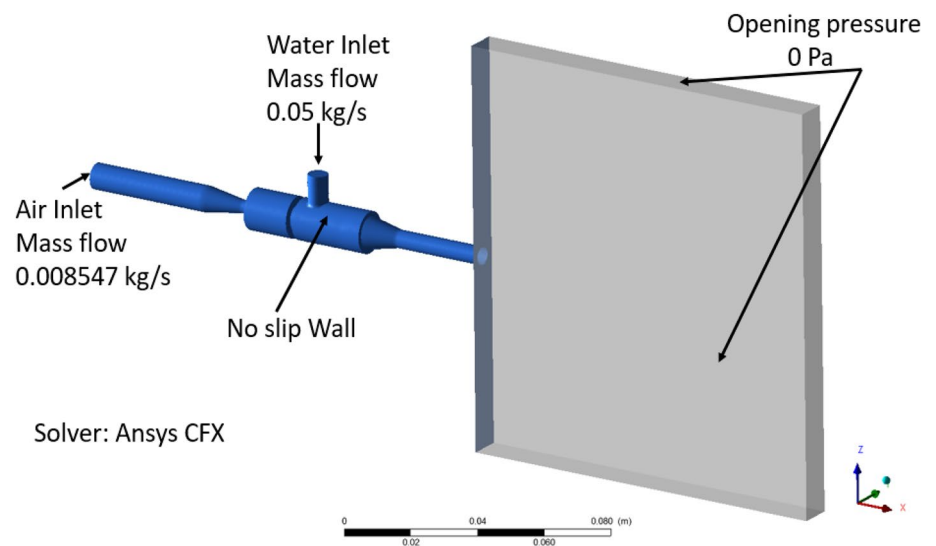**Fig. 2** Schematic representation of the equipment used

Fig. 3 The boundary conditions used to in the ANSYS® CFX simulation

software ANSYS® CFX with the same experimental variables. Therefore, a homogenous multiphase model was used with a standard free-surface model. In this study, it was assumed that the velocity field of the particles was the same as that of the water. The boundary conditions used in the CFD analysis are shown in Fig. 3.

The working pressure was set to 55 psi, and the tests were conducted for approximately 140 s. After a test was finished, the sample was removed from the test apparatus and weighed with a high-precision VIBRA scale, which has a resolution of 0.0001 g; this procedure was carried out 4 times per specimen to measure the rate of wear. The test parameters are shown in Table 1.

As a precaution, the working pressure was checked and adjusted periodically during the tests, and velocity measurements were also collected to ensure test repeatability. The testing design included sufficient randomness to meet the criteria of statistical normality.

Table 1 Constant parameters for the erosion wear experiments

Parameter	Values	Units
Pressure	55	psi
Abrasive amount	100	g
Attack angle	90	Degrees
Particle size	212–300	μm
Test time	2:20	min:seg
Concentration	1.25	wt%

3 Results and Discussion

3.1 Abrasives

Morphology is one of the parameters that influence erosive wear. Therefore, this aspect must be controlled, and the

Fig. 4 Microphotographs of the **a** Al_2O_3, **b** garnet, and **c** silica sand particles
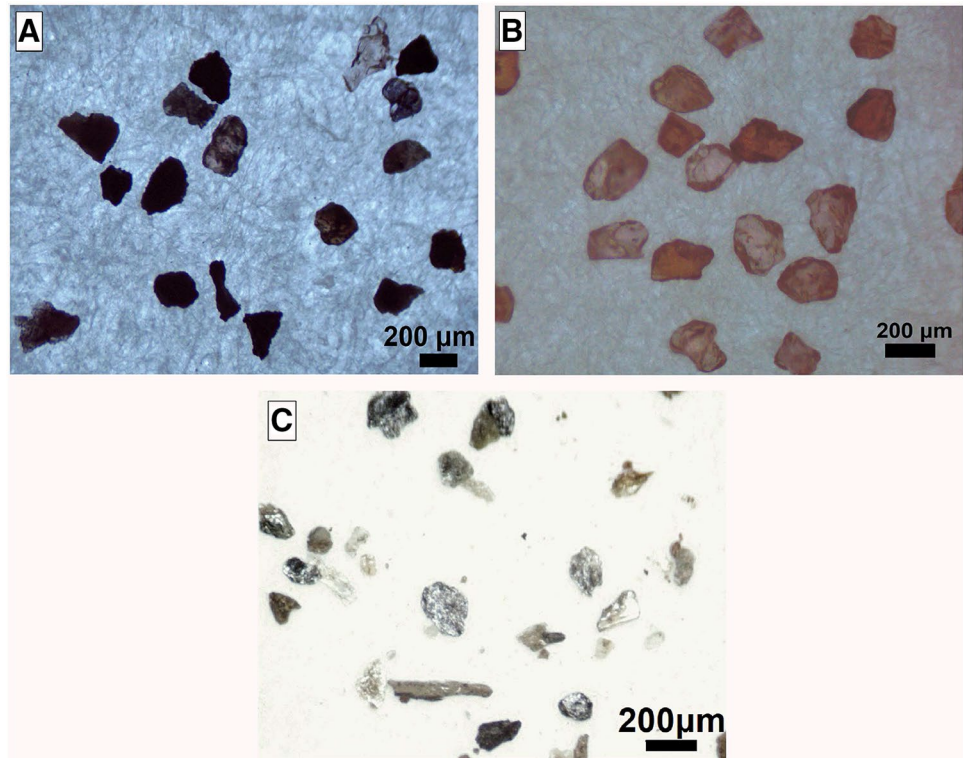

Table 2 Modified shape factor (SF_{Mod}) for the three abrasives used

Abrasive	SF_{Mod}	95% confidence interval
Garnet	0.76	0.01
Al_2O_3	0.78	0.01
Silica sand	0.71	0.04

Table 3 Calculated and reference density for each abrasive

Abrasive	Density (g/cm^3)	Density (g/cm^3) [21]
Al_2O_3	3.91 ± 0.35	3.99
Garnet	3.16 ± 0.12	–
Silica sand	2.13 ± 0.21	2.65

modified shape factor (SF_{Mod}) of each abrasive was calculated based on the photos as shown in Fig. 4.

As shown in Table 2, the SF_{Mod} values obtained for the garnet and Al_2O_3 particles are approximately equal, and a smaller SF_{Mod} was obtained for the silica sand. However, the SF_{Mod} value for the silica sand was very close to those for the other abrasives. In summary, the SF_{Mod} values were very similar between the abrasives; therefore, we could assume that the morphology would not influence the erosion wear tests. This condition will allow us to study the effect of H_a/H_m on erosion without the influence of particle morphology, which is one of the main goals of the present study.

The experimental values for the abrasive densities are shown in Table 3. These measurements are important to perform in erosion wear studies because an abrasive usually contains traces of other elements that alter its true density. This change in density must be considered because the

Table 4 Vickers hardness of the abrasives

Abrasives	Hardness ($HV_{1.96 N}$)	Hardness ($HV_{0.98 N}$) [13]	Hardness (HV) [11]
Al_2O_3	2068 ± 91	2563 ± 124	1800–2000
Silica sand	776 ± 124	–	750–1200
Garnet	1315 ± 50	1453 ± 85	600–1000

momentum carried by particles of various densities differs, affecting the erosion wear phenomenon. The effect of particle density on the erosion wear regimes will be discussed further (see Figs. 7, 8).

Table 4 shows the measured hardness of each abrasive and the hardness reported in the literature. There are some differences in the hardness values of the Al_2O_3 and silica sand, possibly due to the various methods and equipment

Table 5 Vickers hardness of the materials used

Material	Target hardness (HV)	Hardness obtained (HV)
AISI 420	300	299 ± 3
AISI DF2	400	424 ± 7
AISI M2	550	549 ± 4
AISI D2	600	592 ± 4
AISI D3	700	704 ± 7
Cemented carbide	1500	1455 ± 7

Table 6 Hardness ratios: idealized and obtained from the erosion tests

Abrasive and material combination	H_a/H_m obtained	H_a/H_m target
Garnet/cemented carbide	0.90 ± 0.04	1
Silica sand/AISI D3	1.10 ± 0.18	1.1
Silica sand/AISI D2	1.31 ± 0.21	1.3
Silica sand/AISI DF2	1.83 ± 0.32	1.8
Garnet/AISI D3	1.86 ± 0.08	1.9
Garnet/AISI D2	2.22 ± 0.09	2.2
Silica sand/AISI 420	2.60 ± 0.44	2.6
Al$_2$O$_3$/AISI D3	2.94 ± 0.15	3
Garnet/AISI DF2	3.10 ± 0.08	3.5
Al$_2$O$_3$/AISI M2	3.77 ± 0.19	4
Al$_2$O$_3$/AISI DF2	4.87 ± 0.30	5

used to determine the hardness values and the deviation in the chemical composition of any single abrasive.

3.2 Materials

The hardness obtained using the heat treatment is compared with the target hardness in Table 5. The hardnesses achieved in this study closely matched the idealized requirements for the study of the H_a/H_m ratio on erosion wear.

3.3 Wear Tests

The erosion wear tests were performed using eleven H_a/H_m ratios, as shown in Table 6. It is observed that the experimentally obtained H_a/H_m ratios are very close to the values initially proposed. With the values obtained, an accurate assessment of a possible mild-severe wear transition regime is likely.

To construct a graph of the average wear rate (mg/min) as a function of the hardness ratio H_a/H_m, the mass loss (mg) is first plotted vs time (min), as shown in Fig. 5. In all such graphs (which are not all shown because of space
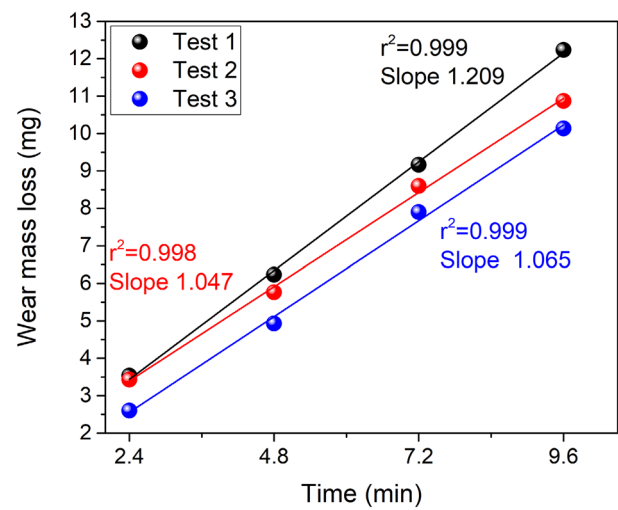

Fig. 5 Wear mass loss as a function of time for the H_a/H_m ratio of 1.31 using silica sand/AISI D2
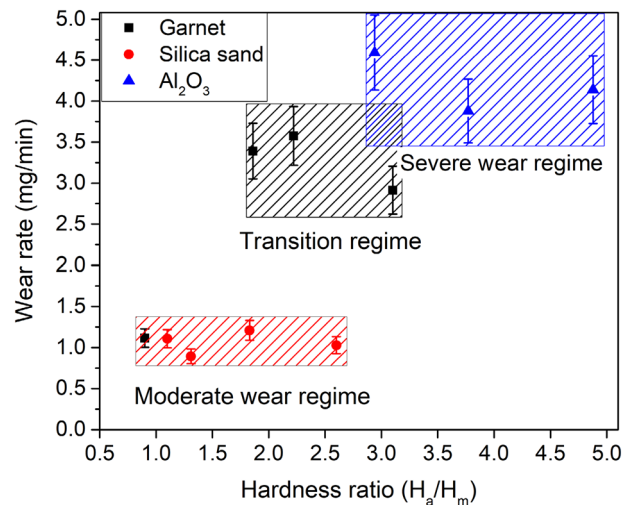

Fig. 6 Erosion wear rate (mg/min) as a function of the H_a/H_m ratio (the bars correspond to the 95% confidence interval)

limitations), the wear mass loss vs. time curve changes linearly, and the slope of the straight line represents the erosion wear rate; the linear relationship indicates that the erosion wear rate was in a steady state. The average erosion wear rate (mg/min) vs. H_a/H_m was plotted in Fig. 6 (the 95% confidence interval of the data shown in Fig. 4 is plotted as error bars in Fig. 5 for each H_a/H_m). The results show that there are three clearly differentiable data groups corresponding to low, medium, and high wear rates. The H_a/H_m ratio is not the only parameter that defines if an abrasive-material pair belongs to one of these groups; this result is different than that of the abrasion behavior reported in [13], in which the

data have low scattering for a specific H_a/H_m value and a clear mild-severe transition is observed.

In the moderate wear regime, the erosion wear rate is approximately constant for H_a/H_m values from 0.9 ± 0.04 to 2.6 ± 0.04, and a small scattering of the wear data is observed, which is expected to occur due to the slight deterioration of the surface in this regime, as will be discussed in the next section. In addition, the low density of the silica sand (see Sect. 3.1) could result in a very low transfer of momentum by the particles as they hit the sample surface, which may help explain the low wear rates. In contrast, in the severe wear regime, the erosion wear rates are nearly four times greater than the moderate wear values. Basically, a greater area (groove size) of the material was affected, and deeper groves were also observed in the severe wear regime than were observed in the other wear regimes (see the next section), creating the broad scattering of the wear data in this regime. Furthermore, the high density of the Al_2O_3 particles (see Sect. 3.1) favored a large momentum transfer from the particles to the sample surface, which produced a high erosion wear rate. Therefore, the particle density could be as important as the hardness in the erosion wear phenomenon. This discussion is schematically represented in Fig. 7.

In addition to the H_a/H_m ratio effect, the density of the abrasive particles and the number of particles that impact the sample surface could also affect the wear response. Therefore, the wear rate values (Fig. 6) were modified to include the effect of the number of particles (which includes the density value) in the wear phenomenon. The number of particles that impacted the surface was calculated, considering the density of the particle and the total mass of the abrasives used and assuming that the abrasives had a spherical geometry with a mean diameter of 250 μm. The number of particles was calculated according to Eq. (5):

$$N_p = \frac{M_a}{V_p * \rho_p} \tag{5}$$

where M_a is the total mass (g) of the abrasives used; ρ_p is the density of a single abrasive particle in g/cm^3, and V_p is the volume (cm^3) of that abrasive particle (spherical shape). This equation allowed the construction of Fig. 8, in which the wear rate was divided by the number of particles
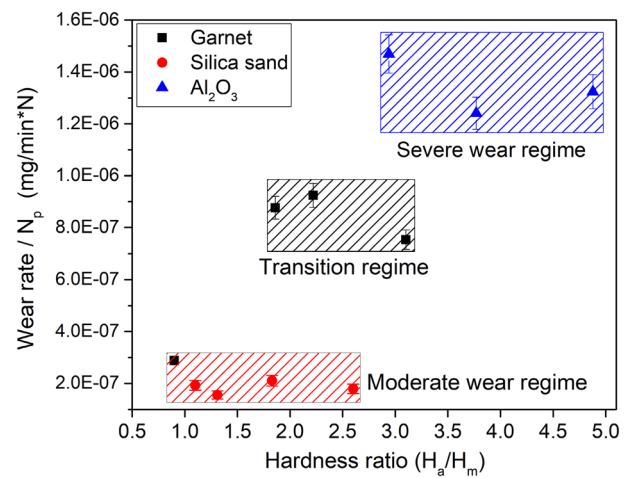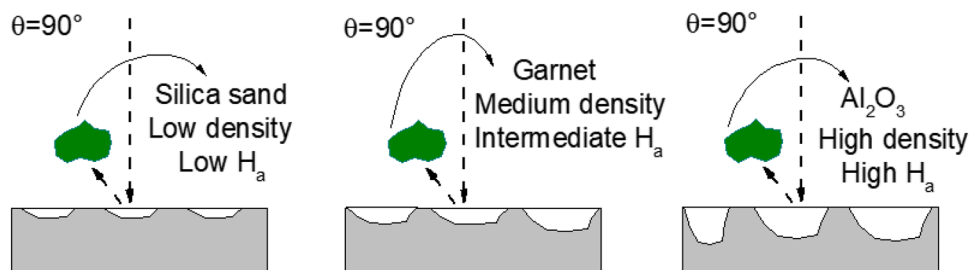

Fig. 8 Erosion wear rate (mg/min) modified by the number of particles (N_p) as a function of the H_a/H_m ratio (the bars correspond to the 95% confidence interval)

impacting the sample surface and plotted as a function of the H_a/H_m ratio.

The first difference between Figs. 6 and 8 to note is that in Fig. 8, the three wear regimes are located farther away from each other in parameter space, meaning that the number of abrasive particles and their density (momentum) has a tangible effect on the erosion wear phenomenon. For instance, at the H_a/H_m ratio of 0.9 ± 0.04 (garnet/cemented carbide), the wear rate per particle is greater than those obtained for the silica sand at other H_a/H_m ratios because of the number of particles used; therefore, their density is considered in the erosion wear result. In other words, despite having the lowest H_a/H_m ratio and fewer particles impacting the sample surface, this wear rate is higher than that of other H_a/H_m ratios in the moderate wear regime because of the high momentum transfer. Finally, a similar analysis was performed for the H_a/H_m ratio of 3 ± 0.15, for which very dissimilar wear rates were obtained despite the consistent hardness ratio; this result can be partially explained by the strong effect of the density (and thus the momentum) of the particles on the erosion wear.

However, a new analysis modification is necessary, as the three regimes still overlap between H_a/H_m ratio values

Fig. 7 Schematic representation of the erosion phenomenon in terms of hardness and momentum, according to the results obtained

of 1.9 ± 0.08 and 3 ± 0.15. This result indicates that some important physical phenomenon must be included in the analysis. In this sense, the fragmentation of the abrasive could be a critical factor in erosion; thus, the particle toughness must be considered. Therefore, the fracture toughness (which is a measurement of the energy required to propagate a crack and thus a measurement of the material resistance to fracture) of the three abrasives was taken into account (Table 7), that is, the fragmentation phenomenon of the abrasives during wear was taken into account through the fracture toughness.

Figure 9 was constructed with the modified hardness ratio (according to the fracture toughness); thus, the link between the conservation of momentum transfer and the fragmentation of the abrasive particles (intrinsic properties of the erodent) was taken into account through this term. Notably, the inclusion of the fracture toughness of the abrasives allows a clear distinction of the three regimes, with no overlap. The severe wear regime is located in the upper right corner of Fig. 9, where the wear rate is the highest. This regime occurs when Al_2O_3 particles are used, that is, the momentum transfer is highly efficient (more damage on the surface is probable), and fragmentation and fracture of the particles are unlikely. These two simultaneous conditions promote the severe surface damage of the material. In contrast, the moderate wear regime is located in the lower left corner of Fig. 9.

To confirm the role of the fracture toughness of the abrasive in the wear transition, particle granulometry curves were generated after the wear tests, using silica sand/AISI D3, Al_2O_3/AISI DF2, and garnet/AISI D3 couples, aiming to confirm that the abrasive with the lowest fracture toughness (silica sand) was fragmented easily during the wear test, while the abrasive with the highest fracture toughness was not. This approach confirmed that the results obtained in Fig. 8 have important significance for the wear transition in erosion wear and can be used in future analyses. The change in abrasive granulometry is observed in Fig. 10.

Figure 10 shows that the silica sand underwent a high degree of fragmentation and reduction of the mean size of the particles during the wear process, as expected due to its low K_{Ic} (Table 7). This behavior produced a reduction in the potential damage to the sample surface by the sand abrasive. In contrast, the alumina abrasive showed limited change in

Table 7 Fracture toughness (K_{Ic}) of selected abrasives

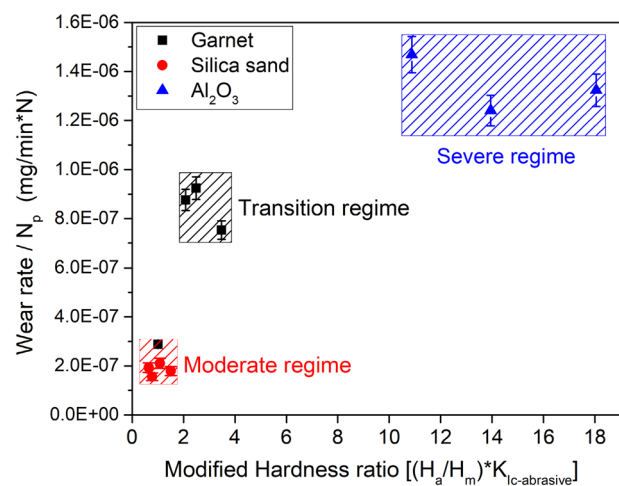| Abrasive	Fracture toughness (K_{Ic} MPa$\sqrt{m}$)	Reference
Garnet	1.12	[22]
Silica sand	0.58–0.60	[23, 24]
Al_2O_3	3.39–3.75	[25]

Fig. 9 Erosion wear rate (mg/min) modified by the number of particles (N_p) as a function of the H_a/H_m ratio modified according to the fracture toughness of the abrasive (the bars correspond to the 95% confidence interval)

granulometry, as expected due to the its high K_{Ic}. The tendency of the alumina abrasive to not undergo fragmentation induced a greater surface damage to the sample. A similar behavior was observed for the garnet abrasive. From these results, it can be concluded that the fracture toughness of the abrasives must be included in the wear transition analysis for a complete understanding of the phenomena that occur.

3.3.1 Wear Surfaces

The erosion wear transition regimes identified in the previous section are related to observations in the wear surfaces.
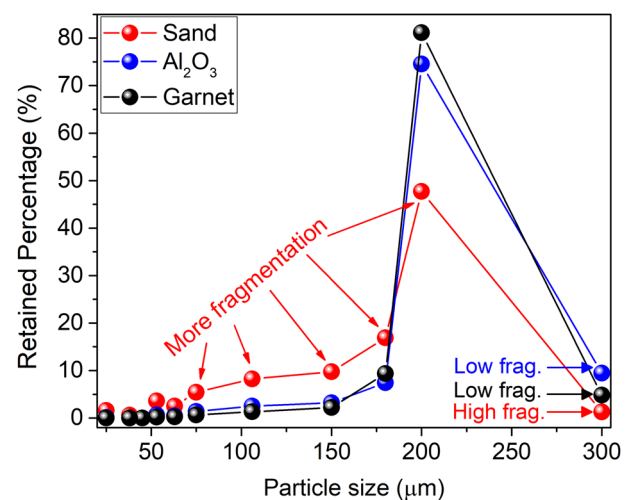

Fig. 10 Change in the abrasive granulometry due to the erosion test, 100% of the abrasives before the test were retained in the 300 µm sieve

$(H_a/H_m)*K_{ic\text{-}abrasive}= 0.65$
Silica sand / AISI D3
Moderate wear regime

$(H_a/H_m)*K_{ic\text{-}abrasive}= 3.47$
Garnet / AISI DF2
Transition wear regime

$(H_a/H_m)*K_{ic\text{-}abrasive}= 18.04$
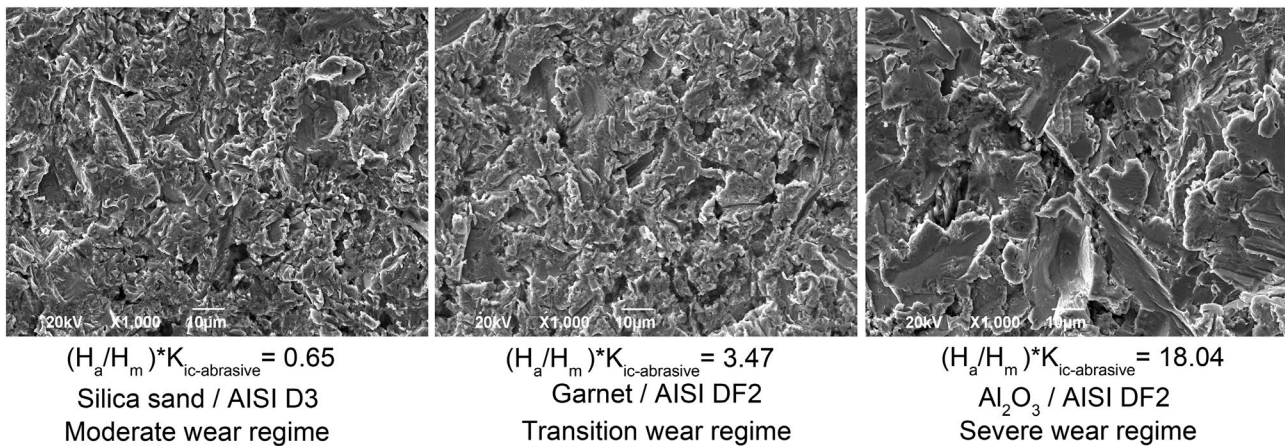Al$_2$O$_3$ / AISI DF2
Severe wear regime

Fig. 11 Representative wear surfaces for the moderate wear regime, transition wear regime, and severe wear regime

Three important conditions were selected to analyze the morphological changes during the increase in the modified H_a/H_m ratio; these changes were identified using a scanning electron microscope. These conditions were representative of the three regimes found in Fig. 9: the moderate wear regime, the transition wear regime, and the severe wear regime. The representative wear surfaces of each regime are shown in Fig. 11.

According to the observations from Fig. 11 (left), a relatively mild/lesser degradation of the wear surface occurs in the moderate wear regime, and this degradation was caused by plastic deformation; furthermore, this relatively small amount of damage supports the erosion wear rates found in this zone. Under this condition, the entire wear surface area was affected, but the cavities produced by the wear are small. An increase in the cavity sizes can be clearly seen in the transition regime as the modified H_a/H_m ratio increases. In the transition regime (Fig. 11 (center)), the wear surface was affected more by the severe plastic deformation caused by the garnet abrasives, as can be inferred by comparing the cavity sizes and the other wear features with those of the other wear regimes. These features support the observed increase in the erosion wear rate. Finally, in the severe wear regime (Fig. 11 (right)), an intense plastic deformation was observed, accompanied by large cavities, and the removal of small areas of material by microcutting and microploughing mechanisms was also observed. These micromechanisms were identified due to the clean-cut features and microchip formation (microcutting) and wedge formation (microploughing). This severe degradation of the surface explains the high rate of wear recorded in the zone of severe wear. Notably, plastic deformation, not microcutting, was the major damage mechanism present in all three regimes. These observations are consistent with the results for ductile materials such as aluminum [26] and stainless steel [7] subjected to high impact angles (90°).

In summary, for the moderate wear regime, only superficial grooves and slight plastic deformation were observed. Similar wear surface features have been reported to dominate at high impact angles and in zones of relatively low wear [27]. Deeper grooves and craters were observed in the transition wear regime than those observed in the moderate wear regime. Therefore, in the transition wear regime, the stress field within the material becomes significant. Finally, in the severe wear regime, the deepest grooves and craters were observed, as were plastic deformation and microcutting.

4 Conclusions

We used three types of abrasives and several types of heat treatments and materials to study the mild-severe wear transition in erosion wear. The major conclusions are summarized as follows:

The use of the abrasive/material hardness ratio as well as the density and the fracture toughness of the abrasives produces a clear distinction between erosion wear regimes. In this regard, a moderate wear regime was observed for abrasive/material hardness ratios modified by the fracture toughness of the abrasive, $H_a K_{Ic\_abrasive}/H_m$, less than 2; additionally, a severe-moderate transition was detected for $H_a K_{Ic\_abrasive}/H_m$ values between 2 and 4. From the wear mechanisms presented in each wear regime, it is possible to summarize that the wear surfaces of the moderate wear regime exhibited relatively little plastic deformation with little surface degradation. In the transition zone, more plastic deformation was observed, whereas in the severe wear regime, plastic deformation, microcutting, and large cavities were observed, degrading the sample surface. The aforementioned results can be applied to the design of hydraulic turbines that are subjected to hard particle wear and to

the selection hardness ratios for which only moderate wear occurs for specific particle types.

References

1. Lindsley, B.A., Marder, A.R.: The effect of velocity on the solid particle erosion rate of alloys. Wear **225**, 510–516 (1999)
2. Desale, G.R., Gandhi, B.K., Jain, S.C.: Effect of erodent properties on erosion wear of ductile type materials. Wear **261**(7), 914–921 (2006)
3. Akbarzadeh, E., Elsaadawy, E., Sherik, A.M., Spelt, J.K., Papini, M.: The solid particle erosion of 12 metals using magnetite erodent. Wear **282**, 40–51 (2012)
4. Zheng, C., Liu, Y., Chen, C., Qin, J., Ji, R., Cai, B.: Numerical study of impact erosion of multiple solid particle. Appl. Surf. Sci. **423**, 176–184 (2017)
5. Finnie, I.: Erosion of surfaces by solid particles. Wear **3**(2), 87–103 (1960)
6. Rawat, A., Singh, S.N., Seshadri, V.: Erosion wear studies on high concentration fly ash slurries. Wear **378–379**, 114–125 (2017)
7. Nguyen, V.B., Nguyen, Q.B., Zhang, Y.W., Lim, C.Y.H., Khoo, B.C.: Effect of particle size on erosion characteristics. Wear **348**, 126–137 (2016)
8. Aponte, R.D., Teran, L.A., Ladino, J.A., Larrahondo, F., Coronado, J.J., Rodríguez, S.A.: Computational study of the particle size effect on a jet erosion wear device. Wear **374–375**, 97–103 (2017)
9. Ji, X., Qing, Q., Ji, C., Cheng, J., Zhang, Y.: Slurry erosion wear resistance and impact-induced phase transformation of titanium alloys. Tribol. Lett. **66**(2), 64 (2018)
10. Rao, P.V., Young, S.G., Buckley, D.H.: A study of the effect of solid particle impact and particle shape on the erosion morphology of ductile metals. J. Microsc. **135**(1), 49–59 (1984)
11. Hutchings, I.M., Tribology: Friction and Wear of Engineering Materials. Arnold, E. (ed). CRC Press (1992)
12. Evans, A.G., Wilshaw, T.R.: Quasi-static solid particle damage in brittle solids—I. Observations analysis and implications. Acta Metall. **24**(10), 939–956 (1976)
13. Coronado, J.J., Rodríguez, S.A., Sinatora, A.: Effect of particle hardness on mild–severe wear transition of hard second phase materials. Wear **301**(1), 82–88 (2013)
14. Pintaude, G., Bernardes, F.G., Santos, M.M., Sinatora, A., Albertin, E.: Mild and severe wear of steels and cast irons in sliding abrasion. Wear **267**(1), 19–25 (2009)
15. Wada, S., Watanabe, N.: Solid particle erosion of brittle materials (part 3). J. Ceram. Assoc. Jpn **95**(1102), 573–578 (1987)
16. Feng, Z., Ball, A.: The erosion of four materials using seven erodents—towards an understanding. Wear **233**, 674–684 (1999)
17. Desale, G.R., Gandhi, B.K., Jain, S.C.: Slurry erosion of ductile materials under normal impact condition. Wear **264**(3), 322–330 (2008)
18. Cox, E.P.: A method of assigning numerical and percentage values to the degree of roundness of sand grains. J. Paleontol. **1**(3), 179–183 (1927)
19. Teran, L.A., Roa, C.V., Muñoz-Cubillos, J., Aponte, R.D., Valdes, J., Larrahondo, F., Rodríguez, S.A., Coronado, J.J.: Failure analysis of a run-of-the-river hydroelectric power plant. Eng. Fail. Anal. **68**, 87–100 (2016)
20. Harry, C., Heat Treaters Guide: Practices and Procedures for Irons and Steels. ASM International, Ohio (1995)
21. Munz, D., Fett, T., Ceramics: Mechanical Properties, Failure Behaviour, Materials Selection, vol. 36. Springer, Berlin (2013)
22. Samuels, L.E., Metallographic Polishing by Mechanical Methods. Asm International, Ohio (2003)
23. Daphalapurkar, N.P., Wang, F., Fu, B., Lu, H., Komanduri, R.: Determination of mechanical properties of sand grains by nanoindentation. Exp. Mech. **51**(5), 719–728 (2011)
24. Harding, D., Oliver, W., Pharr, G., Cracking during nanoindentation and its use in the measurement of fracture toughness. MRS Online Proceedings Library Archive. **356** (1994)
25. Carlton, H.D., Elmer, J.W., Freeman, D.C., Schaeffer, R.D., Derkach, O., Gallegos, G.F.: Laser notching ceramics for reliable fracture toughness testing. J. Eur. Ceram. Soc. **36**(1), 227–234 (2016)
26. Neilson, J.H., Gilchrist, A.: Erosion by a stream of solid particles. Wear **11**(2), 111–122 (1968)
27. Nguyen, Q.B., Lim, C.Y.H., Nguyen, V.B., Wan, Y.M., Nai, B., Zhang, Y.W., Gupta, M.: Slurry erosion characteristics and erosion mechanisms of stainless steel. Tribol. Int. **79**, 1–7 (2014)